The influence of surfactants on dip coating of fibers: numerical analysis.

Journal:	*Industrial & Engineering Chemistry Research*
Manuscript ID	ie-2015-04918r.R2
Manuscript Type:	Article
Date Submitted by the Author:	01-May-2016
Complete List of Authors:	Campana, Diego; INTEC-CONICET; Facultad de Ingeniería - Universidad Nacional de Entre Ríos Ubal, Sebastián; Instituto de Desarrollo Tecnologico para la Industria Quimica; Facultad de Ingeniería - Universidad Nacional de Entre Ríos Giavedoni, María; Instituto de Desarrollo Tecnologico para la Industria Quimica Saita, Fernando; Instituto de Desarrollo Tecnologico para la Industria Quimica

The influence of surfactants on dip coating of fibers: numerical analysis.

Diego M. Campana,[a,b,] Sebastián Ubal,[a,b] María D. Giavedoni,[a] and Fernando A. Saita.[a]*

[a] INTEC (UNL – CONICET), Güemes 3450, 3000, Santa Fe, Argentina.

[b] Facultad de Ingeniería (UNER), Ruta 11 (Km 10), 3100, Oro Verde, Argentina.

* dcampana@santafe-conicet.gov.ar

ABSTRACT

In this work we numerically analyze the process of dip coating on fibers when the liquid to be deposited contains soluble surfactants. The predictions obtained are in excellent agreement with experimental results reported by different authors. Our results show that the thickness of the film deposited, and particularly the so-called surfactant thickening effect, changes its behavior when the coating speed exceeds certain limits; therefore, the effects produced by inertia forces are scrutinized in order to uncover, for the first time, the mechanisms inducing those changes.

KEYWORDS dip coating, cylindrical fibers, surface active agents, finite elements.

1. INTRODUCTION

When a fiber is withdrawn out of a liquid bath with constant speed, V, it can eventually entrain a liquid film of constant thickness, e. This thickness is determined by the interplay of

viscous, inertia, surface and gravity forces and the process is known as dip coating, a process of crucial importance for example, in the manufacture of optical and textile fibers. As in many other coating processes,[1] the question of practical importance is to predict the value of e.

The first answer to this question was proposed by Landau and Levich[2] and Deryagin,[3] who evaluated the thickness of the film formed when a solid plate is slowly pulled out of the bath. They assumed that the flow can be divided in three regions: the static meniscus at the bottom, a film of constant thickness on top, and in-between the dynamic meniscus where the film is formed. The value of e is determined by matching asymptotically the static and dynamic menisci and the solution is known as the Landau-Levich-Deryagin law (LLD for short). This analysis can be readily extended to small cylindrical fibers by changing the value of the static curvature at the matching point.[4] As result, a simple expression known as the "LLD law" for the fluid thickness coating the fiber was derived: $e_{\mathrm{LLD}} = 1.34\, bCa^{2/3}$. Here, b represents the fiber radius and $Ca = \mu V/\sigma_0$ is the capillary number, μ being the fluid viscosity, and σ_0 the surface tension. Since this study, a considerable amount of work has been published to analyze the effects of gravity, inertia, and Marangoni stresses (among others) on the process. Quéré presents an excellent review of the research and literature addressing this problem,[5] also chapter 13 of the book of Kistler & Schweitzer[1] considers several technological aspects of the process, including solvent evaporation and microstructure control of the deposited film.

A large number of studies regarding the action of surfactants on the problem were published by Quéré and co-workers.[6-8] These authors have carried out experiments to evaluate the effects of surface active agents on the film thickness. The experiments show that the surfactants give rise to a thicker film than that formed in the corresponding clean system. There are two mechanisms by which surfactants modify the film thickness: (i) the reduction of the equilibrium interfacial tension σ_0 —which results in an increase in the capillary

number *Ca*— and (ii) the effect of Marangoni stresses arising from a non-uniformity of the surface tension. To take into account only the last effect, it is customary to define a thickening factor[6] α as the ratio between the measured film thickness and the one predicted by the LLD law, the latter calculated using the equilibrium surface tension (see Equation (13) below). The fibers used in the experiments of Quéré and co-workers have radii equal to 88.5μm and 12.5 μm, and they are pulled out of a solution with concentration of surfactant above the critical micellar concentration; the solution is trapped in a capillary tube of 4 mm diameter and 10 cm long. The coating speed is varied so that the capillary number is within the range 10^{-3}-10^{-2}.

Their results for aqueous solutions of SDS (sodium dodecyl sulfate) show that the thickening factor α is constant and equal to 1.8±0.1 or 2.4±0.1 for the thicker and the thinner fiber, respectively, when the Weber number ($We = \rho V^2 b/\sigma_0$) is smaller than 1 (i.e., in the region where inertia is negligible). Also, values of α remain constant for concentrations between 1 and 9 times the critical micellar concentration (cmc).

To understand better the effects of the surfactant solubility on α, these authors also carried out experiments with a family of cationic surfactants (the *n*-TAB) where the length of the carbon chain changes from *n*=10 to *n*=16: as *n* increases the water solubility of the surfactant diminishes and thus its affinity for the interface increases. For *n*=14 and *n*=16, the trend followed by the film thickness within the range of capillary numbers explored is similar to that reported for SDS: that is, α is constant. However, for *n*=10 and *n*=12 (i.e. for larger solubilities), this trend depends on the surfactant concentration. At relatively low concentrations (of the order of 1 cmc), α is independent of the capillary number as reported previously, but at larger concentrations the behavior changes. For the lower speeds considered in the experiments, the thickening factor is constant but as *Ca* is increased α slowly diminishes and seems to approach a value slightly larger than 1. In a more recent

paper, Scheid et al.[9] show, both theoretical and experimentally, that surface viscosity has also a film thickening effect that can persist even for capillary numbers for which Marangoni stresses are negligible.

Similar results to those of Quéré[6] were reported by Shen et al. in their experiments.[10] They measured the thickness of the film on a fiber withdrawn from solutions of different surfactants (SDS, Triton X-100, and protein bovine serum albumin).

An approximate model of the problem was presented by Park[11] who studied the case of a solid plate pulled out of a liquid bath covered with an insoluble surfactant at very low coating speeds. The results of this analysis show that surfactants affect the film thickness of the entrained film within a range of capillary numbers that depends on the magnitude of the elasticity number, a parameter that expresses how rapidly surface tension varies with the interfacial concentration of surfactant. In fact, the thickening factor is a non monotonic function of the capillary number: at very low coating speeds surface diffusion is large enough to erase the concentration gradients while at high coating speeds, viscous forces overcome the elastic forces due to surface tension gradients, therefore, at both ends the film thickness can be calculated with the LLD law, according to Park's model. In between those extremes, α first increases and then decreases as the capillary number is augmented. The largest value attained by α is $4^{2/3}$ that is also the maximum value reported in the experiments carried out by Quéré and de Ryck.[8] This limit was first proposed by Carroll and Lucassen[12] assuming that the free surface behaves as a solid, and was predicted later by Ratulowski and Chang[13] in their analysis about the effect of soluble surfactants on the thickness of the film left behind by a large bubble displacing a liquid in a capillary tube.

In the last decade, an important number of investigations on the effect of surfactants on plate coating have been published.[14, 15] For this planar geometry, the analyses of the effects of both soluble and insoluble surfactants on the dip coating process based on the solution of the

full hydrodynamic problem have been published;[16, 17] however, up to our knowledge, there is not a similar analysis when the solid withdrawn from the liquid is a cylindrical fiber. The objective of this work is two-fold. The first one is to numerically reproduce the experiments reported by Quéré and de Ryck to validate our numerical procedure.[8] The second one is to gain a better comprehension about the effects of the surfactant on the dip coating of small cylindrical fibers, focusing the analysis in the visco-inertial regime. To that end, continuity and Navier-Stokes equations coupled to the interfacial mass balance of surfactant are numerically solved in steady state. The concentration of solute in the bulk is assumed constant and the exchange of surfactant between the bulk and the interface takes place by an adsorption process that follows Langmuir-Hinshelwood kinetics. The dependence of surface tension on the interfacial concentration of surfactant is modeled by Frumkin's isotherm.

2. MATHEMATICAL FORMULATION

A cylindrical fiber of small radius, b, is vertically withdrawn with constant velocity, V, of a large liquid bath (see Figure 1). The liquid is Newtonian with constant density, ρ, and viscosity, μ, the air above it is inviscid and its pressure is arbitrarily set equal to zero. The coating liquid is an aqueous solution of surfactant whose concentration in the bulk phase, C_0, is very large and thus it is assumed constant. When the interface is at equilibrium with the bulk, the surface concentration of surfactant is equal to Γ_0, and the surface tension is equal to σ_0. The flow, which is assumed stationary in this work, is then governed by continuity and Navier-Stokes equations which in the coordinate system adopted (Figure 1) are

$$\frac{\partial v}{\partial r} + \frac{v}{r} + \frac{\partial u}{\partial z} = 0\,, \tag{1}$$

$$ReCa\left(v\frac{\partial v}{\partial r} + u\frac{\partial v}{\partial z} \right) = -\frac{\partial p}{\partial r} + Ca\left[\frac{\partial}{\partial r}\left(\frac{1}{r}\frac{\partial (r\,v)}{\partial r} \right) + \frac{\partial^2 v}{\partial z^2} \right] \tag{2}$$

$$ReCa\left(v\frac{\partial u}{\partial r}+u\frac{\partial u}{\partial z}\right)=-\frac{\partial p}{\partial z}+Ca\left[\frac{1}{r}\frac{\partial}{\partial r}\left(r\frac{\partial u}{\partial r}\right)+\frac{\partial^2 u}{\partial z^2}\right]-Bo\,. \tag{3}$$

Equations (1) - (3) are dimensionless; u and v are the velocity components in the z- and r-directions, respectively. The characteristic scales are V for velocities, b, for length, and (σ_0/b) for pressure. In the above expressions, $Re=\rho bV/\mu$ is the Reynolds number, $Ca=\mu V/\sigma_0$ is the capillary number, and $Bo=\rho gb^2/\sigma_0$ is the Bond number. These equations are solved using the following boundary conditions.

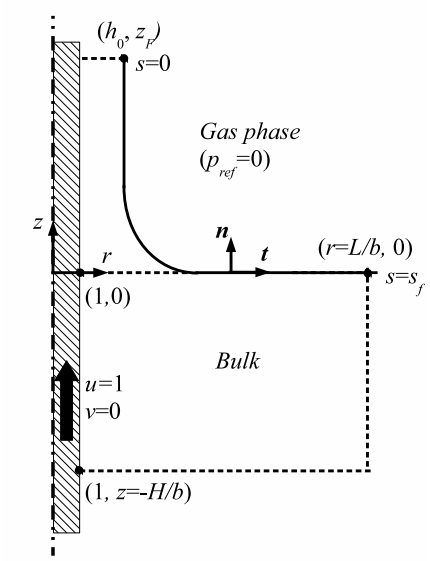

Figure 1: Sketch of the flow domain and coordinate system adopted.

The fluid adheres to the moving fiber; therefore, u=1 and v=0 at r=1. At the film exit boundary located far away from the meniscus (z=z_F), the flow becomes unidirectional and does not change in the axial direction. Thus, the traction vector is

$$\mathbf{T}\cdot\mathbf{e}_z=-p\mathbf{e}_z+Ca\frac{\partial u}{\partial r}\mathbf{e}_r\,, \tag{4}$$

where $\mathbf{T}=-p\mathbf{I}+Ca\left[\nabla\mathbf{v}+(\nabla\mathbf{v})^T\right]$. At the bottom of the domain, z=- H*=-H/b, r>1, the flow does not change along z and the pressure is set equal to its hydrostatic value in the normal component of the stress; therefore, we impose:

$$\mathbf{T}\cdot\left(-\mathbf{e}_z\right) = Bo\,H^*\mathbf{e}_z - Ca\frac{\partial u}{\partial r}\mathbf{e}_r . \tag{5}$$

At the lateral boundary of the domain which is located at a distance L^* far enough from the fiber, we assume that the flow is in the radial direction and the pressure is mainly hydrostatic. Thus, the traction vector is

$$\mathbf{T}\cdot\mathbf{e}_r = \left(Bo\,z + 2Ca\frac{\partial v}{\partial r}\right)\mathbf{e}_r + Ca\frac{\partial v}{\partial z}\mathbf{e}_z . \tag{6}$$

The free surface is a material surface; therefore the usual form of the kinematic condition applies, that is

$$\mathbf{v}\cdot\mathbf{n} = 0 , \tag{7}$$

n being the unit normal vector to the free surface pointing toward the gas phase. We assume that the interface is Newtonian and that the adsorbed surfactant only modifies the surface tension coefficient (i.e. surface viscosity is negligible). Thus, the traction vector at the free surface results

$$\mathbf{n}\cdot\mathbf{T} = \frac{d}{ds}\left(\hat{\sigma}\,\mathbf{t}\right) - \hat{\sigma}\left(\frac{\mathbf{e}_r\cdot\mathbf{n}}{r_{FS}}\right)\mathbf{n} , \tag{8}$$

where $\hat{\sigma}$ is the dimensionless surface tension measured in units of σ_0, **t** is the unit vector tangent to the free surface pointing in the direction of increasing arc length, s (see Figure 1), and r_{FS} is the local radius of the free surface. When a surfactant is present in the system, surface tension is a function of the local concentration of surfactant adsorbed at the interface; therefore, in order to evaluate $\hat{\sigma}$ we need to compute the concentration of surfactant along the free surface and choose an appropriate relationship between this variable and surface tension. The interfacial concentration of surfactant depends on surface diffusion, surface

convection, and the mass exchange process with the bulk according to the following expression,

$$\nabla_s \cdot (\gamma \mathbf{v}_s) - Pe_s^{-1} \frac{d^2\gamma}{ds^2} = j_n . \quad (9)$$

In Equation (9) $\mathbf{v}_s$ is the free surface velocity, γ is the interfacial concentration of the surfactant measured in units of the equilibrium concentration, Γ_0, $Pe_s = bV/D_s$ is the surface Péclét number, D_s being the surface diffusion coefficient of the surfactant, and $\nabla_s \equiv (\mathbf{I} - \mathbf{nn}) \cdot \nabla$ is the surface gradient operator. The mass exchange of solute between the bulk and the interface is carried out by an adsorption/desorption process described by Langmuir-Hinshelwood (L-H) kinetics,[18] which in dimensionless form reads

$$j_n = \frac{St}{l_p}(1-\gamma) , \quad (10)$$

where $St = k_a \Gamma_\infty / V$ is the Stanton number, k_a being the adsorption kinetic constant and Γ_∞ the saturation adsorption concentration, and $l_p = \Gamma_0 / (bC_0)$ is the dimensionless sorption length, a measure of the (in)solubility of the surfactant. Once the interfacial concentration of the surfactant is known, the surface tension can be evaluated. To that end we use Frumkin's equation that in dimensionless form is

$$\hat{\sigma} = 1 + \beta \ln(1 + La - La\gamma) . \quad (11)$$

In Equation (11), $\beta = RT\Gamma_\infty / \sigma_0$ is the elasticity number and $La = k_a C_0 / k_d$ is the Langmuir number, k_d being the desorption kinetic constant.

To complete the formulation of the problem we need to specify boundary conditions for the free surface and for the surface concentration of surfactant. We assume that at $s=s_f$, i.e. far away from the fiber, the free surface is flat and there is equilibrium between the bulk and the

adsorbed surfactant; on the other end (s=0), the free surface is parallel to the moving fiber and the solute concentration does not change along the axial direction; that is,

$$\mathbf{t} = \mathbf{e}_r,\ \gamma = 1 \text{ at } s = s_f, \text{ and } \mathbf{t} = \mathbf{e}_z,\ \frac{\partial \gamma}{\partial s} = 0 \text{ at } s = 0. \tag{12}$$

In the next Section we briefly describe the numerical procedure used to solve problem.

3. NUMERICAL METHOD

The system of equations and boundary conditions (1)–(12) is discretized with the Galerkin / Finite Element Method. Since the flow domain is unknown *a priori*, it has to be simultaneously obtained along with the flow field. For that purpose we use an Arbitrary Lagrangian Eulerian (ALE) formulation, which essentially consists in computing a Winslow's mapping between a fixed reference domain and the physical domain. In order to save computational resources, the mapping is only computed for the flow region near to the free surface; the rest of the flow domain remains equal to the fixed reference domain. A more detailed description of this numerical technique can be found in Campana et al.;[19] here we restrict ourselves to a brief summary of its salient features.

The computational domain is tessellated into an unstructured mesh using triangles. The velocities are approximated with biquadratic Lagrangian basis functions and the pressure is approximated by bilinear Lagrangian basis functions; that is, we use P2P1 Lagrange elements. The interfacial concentration of surfactant is interpolated using the one dimensional specialization of the biquadratic basis functions. We use the divergence theorem to integrate by parts the surface diffusive term of the mass balance of solute (Equation (9)); thus boundary conditions at s=0 are imposed in the weak form. The residuals are built in the usual form (see Campana and Saita[20] for a detailed description of the residual expressions) and in this way a set of non-linear algebraic equations is obtained. This set is simultaneously solved by Newton's method and a direct algebraic solver is used at each iteration step.

To establish the accuracy of the numerical solutions we carried out computations in which the size of the flow domain as well as the size and distribution of the elements within the mesh were varied. From these tests, we established that a domain with z_f=200, r=L/b=1000, and z=H/b=1000 (see Figure 1) is adequate when the coating speed is low; however, when inertia forces become important, the outflow boundary should be located at z_f=400 to obtain a uniform film thickness. In this last situation, the system has around 2,000,000 degrees of freedom. The numerical algorithm described was implemented with the commercial software COMSOL Multiphysics.

4. SOLUTIONS AND DISCUSSION

Our first goal is to reproduce some of the experiments reported in the literature for fiber coating with aqueous solutions of Sodium Dodecyl Sulfate (SDS). To this end we defined the following reference case (RC): the concentration of the SDS solution is equal to 72 mM, i.e. 9 times the critical micellar concentration, the viscosity and density of the solution are 10^{-3} Pa s and 10^3 kg/m^3, respectively, and its surface tension is 0.040 N/m;[8] the surface diffusion coefficient of the surface active agent is D_s=8×10^{-10} m^2/s and its interfacial saturation concentration is $\Gamma_\infty = 10^{-5}$ mol/m^2. The fiber has a radius b=88.5 μm. As we have mentioned in the previous Section, we assume that the mass exchange of solute between the bulk and the interface is carried out by a sorption process described by Langmuir-Hinshelwood kinetics; strictly speaking, this expression, along with Langmuir's isotherm, are considered valid for concentrations below and up to the cmc, not above. Equation (10) could however be seen as a linear expansion of the surfactant flux as Γ departs from its equilibrium value, even when the bulk concentration is above the cmc. This is the approach taken in this work, where value of the kinetic constants will define the slope of this linear expansion. Published values of these kinetic constants show not only large variations with the concentration of the surfactant but also a large scatter for nearly equal concentrations, always

below the cmc.[10,18] To overcome this problem we performed computations to adjust the value of the adsorption kinetic constant, $\hat{k}_a = k_a \Gamma_\infty$ with one of the experimental results presented by Quéré and de Ryck[8] for the same values of the parameters as in the reference case. Following the data published by Chang and Franses,[18] the ratio $\hat{k}_a / k_d$ is set equal to 10^{-6} m in the computations, which also determines that $\Gamma_0 = 8.78\times10^{-6}$ mol/m^2. The experiment selected was taken from figure 53 of Quéré and de Ryck's paper and pertains to the region where the thickening factor is constant and equal to 1.8±0.1; in our computations we set Ca=0.001 and $\hat{k}_a$ was varied until the condition α=1.7 was met, with α defined as follows

$$\alpha \equiv \frac{h_\infty}{h_{\infty,\mathrm{WT}}}, \quad h_{\infty,\mathrm{WT}} = \frac{1.34Ca^{2/3}}{1-1.34Ca^{2/3}}. \tag{13}$$

The reason by which this criterion was established will become apparent when analyzing the results of Figure 3 below. In Equation (13), $h_\infty = e/b$ is the dimensionless film thickness deposited, $h_{\infty,\mathrm{WT}}$ is the prediction of h_∞ obtained by White & Tallmadge[21] for pure liquids (i.e. α=1) when Ca is larger than the range of validity of the LLD law.

The resulting value of the adsorption kinetic constant is $\hat{k}_a = 10^{-3}$ m/s ; hence, values of the dimensionless numbers for the reference case and V=0.04 m/s are: Re=3.54, Pe_s= 4425, β=0.608, St=0.025, La=7.2, and l_P=0.00137.

4.1. The thickness of the entrained film. Influence of coating speed, fiber radius and adsorption kinetic constant

In Figure 2 we show computed values of the film thickness as a function of Ca for the reference case (identified with circles) and when both elastic and inertia forces are neglected (triangles). For comparison, we also depict the measurements reported in Figure 53 of Quéré

and de Ryck's work[8] (squares) and values calculated with the expression proposed by White and Tallmadge;[21] that is Equation (13) with $\alpha = 1$ (WT, continuous line). It is worthy to note, that the physical variable that changes in both the computations and the experiments is the coating speed; therefore, all the dimensionless numbers that depend on this variable change accordingly. The agreement between predictions and measurements is quite good up to $Ca \approx 0.01$ ($V \approx 0.4$ m/s), that is in the visco-capillary regime, but they diverge for larger coating speeds, that is in the visco-inertial regime. This divergence was already noticed in a previous work[19] and it was attributed to the flow reduction caused by the walls of the capillary used as liquid reservoir. This hypothesis is also supported by the preliminary numerical results that we obtained when varying the gap between a fiber and the inner wall of a capillary tube from which the former is withdrawn.[22]

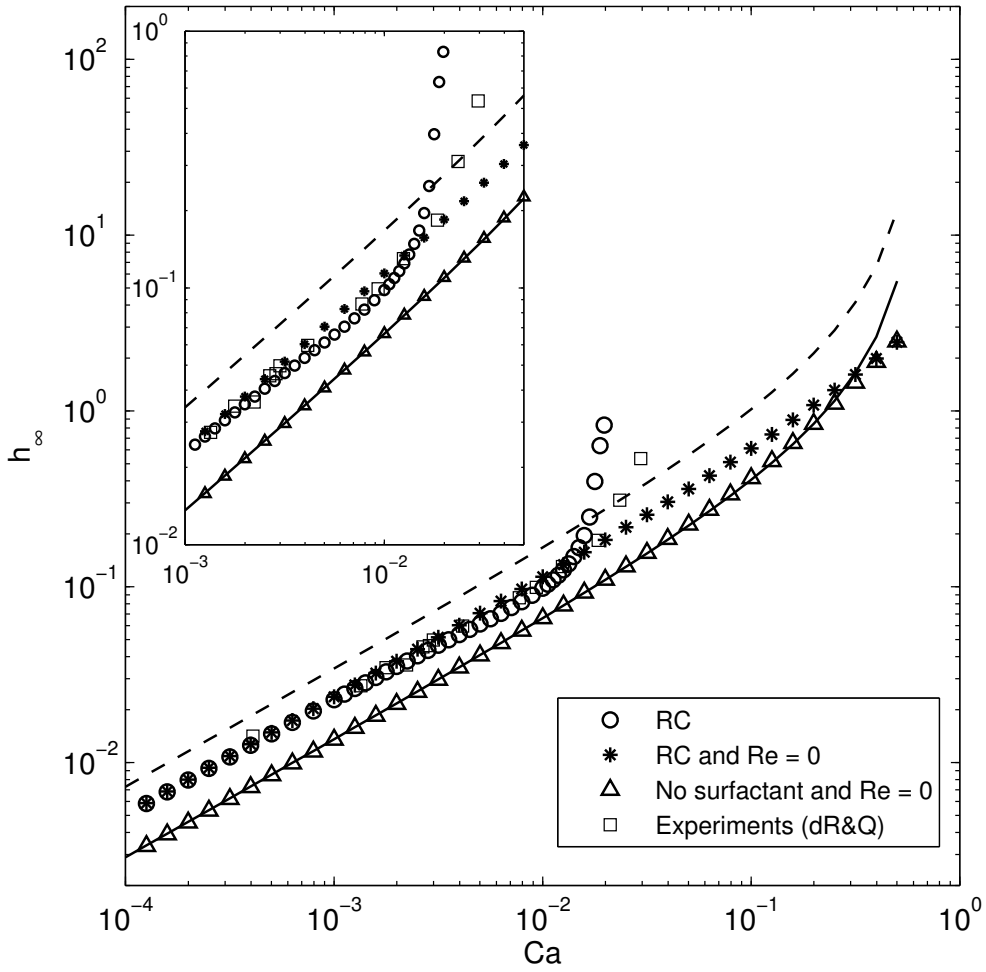

Figure 2: Computed values of the film thickness for RC (circles), the corresponding system with *Re*=0 (asterisks), and measurements reported by Quéré & de Ryck[8] (squares). The solid line corresponds to predictions of WT and the dashed one to a thickening factor $\alpha = 4^{2/3}$.

As the free surface is stretched the surfactant molecules adsorbed at the interface become apart from each other. The concentration gradients thus generated give rise to surface tension gradients and hence to Marangoni tractions which are responsible for the film thickening. On the other hand, surface diffusion and the sorption process are the mechanisms that try to restore a uniform interfacial concentration. To explain the results illustrated in Figure 2, Quéré and De Ryck[8] took into account the order of magnitude of the characteristic time of each process; that is, the residence time of the surfactant in the dynamic meniscus, τ, the

adsorption time, τ_a, and the diffusion time, τ_d. The former depends on the coating speed, V, and on the length of the dynamic meniscus, $l_d \sim b\ Ca^{1/3}$, hence $\tau \propto bCa^{1/3}/V = \mu b/\left(\sigma Ca^{2/3}\right)$. They estimated the adsorption time as the ratio between the equilibrium interfacial concentration of surfactant (Γ_0) and the magnitude of the adsorption flux (j_n), and for this quantity they used the following approximation: $j_n \approx \hat{k}_a C_0 Ca^{2/3}/\beta La$. Since the bulk concentration of surfactant is assumed constant, the relevant diffusion process is the diffusion of the surfactant along the free surface, that is $\tau_{Sd} \propto l_d^{\,2}/D_S$. Within the range of coating speeds considered in Figure 2, the diffusion time is much larger than the residence time, thus surface diffusion has negligible effects on the interfacial distribution of the surface active agent. Moreover, it is easy to see that the ratio between the residence and the adsorption times is finite and independent of the coating speed; this result is in agreement with the region of constant thickening factor detected between $Ca = 10^{-4}$ (i.e., the smallest value considered in this work) and approximately 0.01. Finally, it is important to test the validity of assuming a constant bulk concentration. We estimate the time that takes to a surfactant molecule to diffuse a "penetration" length beneath the surface by $\tau_{Bd} \propto (\Gamma_0 / C_0)^2/D_B$. Assuming $D_B \approx D_S$ and using the values of the reference case, it is easy to see that the bulk diffusion time is two orders of magnitude smaller than the typical adsorption time (tens of microseconds versus milliseconds, respectively). We therefore confirm the validity of our assumption.

If the radius of the fiber diminishes, the residence time is shorter and the adsorption process becomes less effective, therefore, the region of constant thickening factor will be characterized by a larger α as can be observed in Figure 3 where numerical solutions for values of b between 12.5 μm and 225 μm are depicted. The other parameters are those of the reference case, with V=0.04 m/s. In order to estimate the sensitivity of the numerical solution

to variations of the adsorption kinetic constant, we set $\hat{k}_a = 10^{-3}$ m/s (curve labeled RC in Fig. 3) and $\hat{k}_a = 10^{-4}$ m/s (curve labeled C1 in Fig. 3). In this figure we also depicted the experimental thickening factors reported by Quéré and de Ryck for comparison.[8] Clearly, the numerical results obtained for both $\hat{k}_a = 10^{-4}$ m/s and $\hat{k}_a = 10^{-3}$ m/s agree reasonably well with the experimental data, which suggests that any value of $\hat{k}_a$ in between is a reasonable estimation for this quantity within the range of parameters analyzed in this work; therefore, we adopted $\hat{k}_a = 10^{-3}$ m/s as stated above.

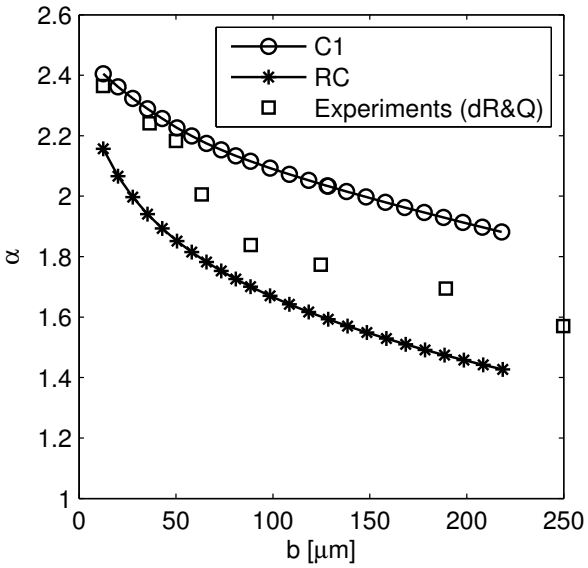

Figure 3: Film thickening factor as a function of the radius of the fiber for two values of the adsorption constant; other parameters are those of the reference case, with $Ca = 0.001$. The squares indicate the experiments of Quéré and de Ryck.[8]

The computed h_∞ values reported in Figure 2, show that α presents a minimum near Ca=0.008; that is in the region where the visco-capillary regime merges into the visco-inertial regime. A similar trend is detected in Figure 4 where numerical predictions of the film thickness as a function of Ca (i.e. the coating speed) are compared with the measurements carried out by Shen et al.;[10] in these solutions, the fiber radius is equal to 38 μm, the bulk

concentration of surfactant is C_0=17 cmc, V is varied in order to cover the experimental range of Ca, and the rest of the physicochemical parameters are as in RC, i.e. no new adjustment of the kinetic constants is made. Also in this case, we notice a good agreement between experiments and numerical predictions.

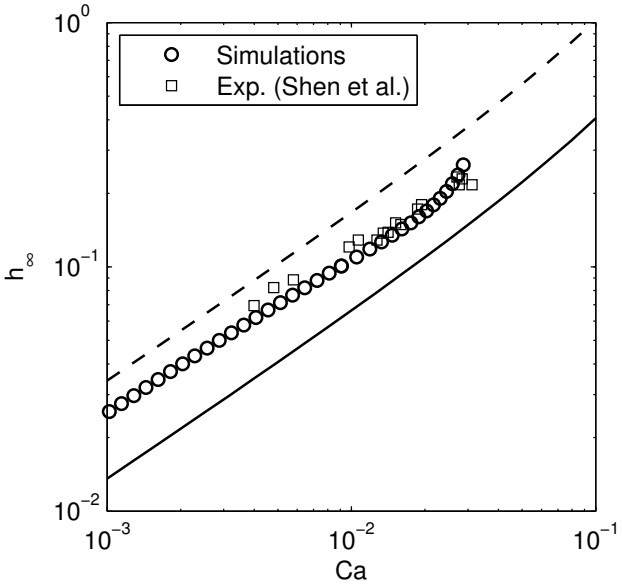

Figure 4: Comparison between numerical predictions (circles) and the measurements by Shen et al. (squares).[10] The solid line corresponds to predictions of WT and the dashed one to a thickening factor $\alpha = 4^{2/3}$.

It could be argued that the minimum in the thickening factor results from an increase of the relative importance of viscous forces respect to the elastic effects of the surfactant at this Ca number. However, numerical solutions for Re=0 (i.e. creeping flow limit, asterisks in Figure 2) do not show this non-monotonic behavior; in fact, the thickening factor is either constant or a decreasing function of Ca, and in the vicinity of Ca=0.008 (that is, at the point where this variable presents a minimum when $Re\neq0$), the thickening factor (α=1.71) is larger than in the RC (α=1.45). This result assures that the inertial effects, though incipient, must be responsible of the non-monotonic behavior observed. In an attempt to disclose the

mechanism by which the inertia forces change the final film thickness, we next analyze several interfacial variables.

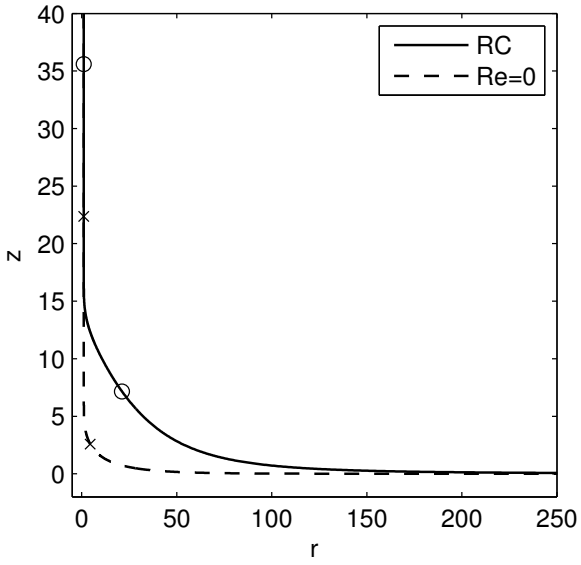

Figure 5: Shapes of the menisci for RC and the corresponding system with *Re*=0. Circles and crosses indicate the approximate limits of the dynamic meniscus for *Re*=28.32 and *Re*=0, respectively.

4.2. Analysis of interfacial variables for the reference case

Figure 5 depicts the interfacial shapes near the fiber for the RC and its counterpart with *Re*=0; in both cases the coating speed is equal to 0.32 m/s (*Ca*=0.008). It is easy to note that inertia significantly changes the shape of the menisci; however, it is well known since the first publications of LLD that the region responsible for the amount of liquid entrained by the fiber is the so called dynamic meniscus (DM); therefore, the interfacial variables must be analyzed there. The limits of the dynamic meniscus — i.e. where the DM matches the static meniscus or where it merges into the film region— are indicated with crosses or circles for *Re*=0 and 28.32, respectively. These limits were established detecting the interfacial points at which the interfacial pressure gradient becomes almost zero (smaller than 10^{-3}); that is, at the points (see Figure 6) where the interfacial pressure p_s becomes zero (matching between DM

and the static meniscus) or equal to $\hat{\sigma}/r_{FS}$ (matching between DM and the film). From both figures, we also find that the length of DM (l_d) is larger when inertia forces are not negligible: in fact, l_d increases from nearly 20 to about 29 (in units of z) or from ~20 to ~40 (in units of s). Since the dynamic meniscus is the region mostly affected by surface stretching, any change of its length should impact the mass transport process. In fact, Figure 7 shows that the interfacial concentration of surfactant not only departs from equilibrium along a larger distance but also its gradients are bigger when inertia forces are considered. Both curves are in agreement with the characteristics presented by the surface velocity for the two cases studied (see Figure 8). For instance, the minimum in surface concentration is at the location where the gradient of surface velocity has a maximum.

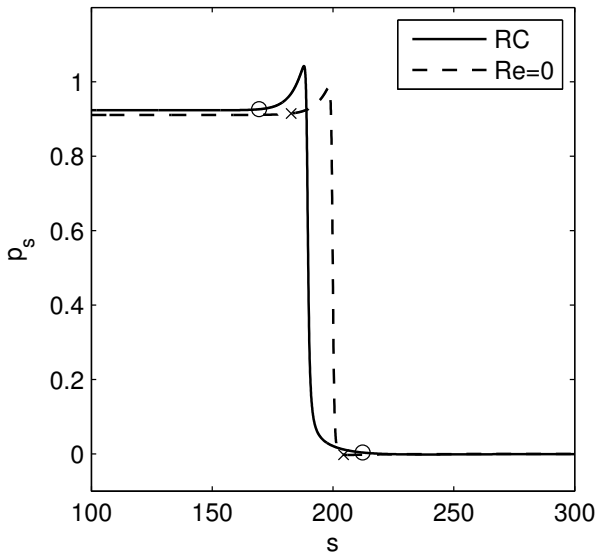

Figure 6: Dimensionless interfacial pressure along the free surface when Ca=0.008 for RC and the corresponding case with Re=0. Circles and crosses indicate the approximate limits of the dynamic meniscus for Re=28.32 and Re=0, respectively.

The surfactant distributions depicted in Figure 7 give rise to Marangoni stresses which are evaluated as $T_{ns} = 1/Ca\left(\nabla_s \hat{\sigma}\right)\cdot \mathbf{t}$ (see Equation (8)) and illustrated in Figure 9; these stresses should be responsible for the local minimum that the thickening factor displays near

Ca=0.008, both in the experiments and in the simulations shown in Figure 2. Considering that the unit tangent vector is directed from the film toward the bulk (see Figure 1) it is easy to note that in the region where these stresses are positive the liquid tends to be dragged from the film towards the bulk while in the region where they are negative the liquid tends to be dragged in the opposite direction. Results depicted in Figure 9 suggest that the tendency to drag liquid toward the bulk is greater when inertia forces are present; thus, they could induce the decrease in α (compared to the case with *Re*=0) reported in Figures 2 and 4.

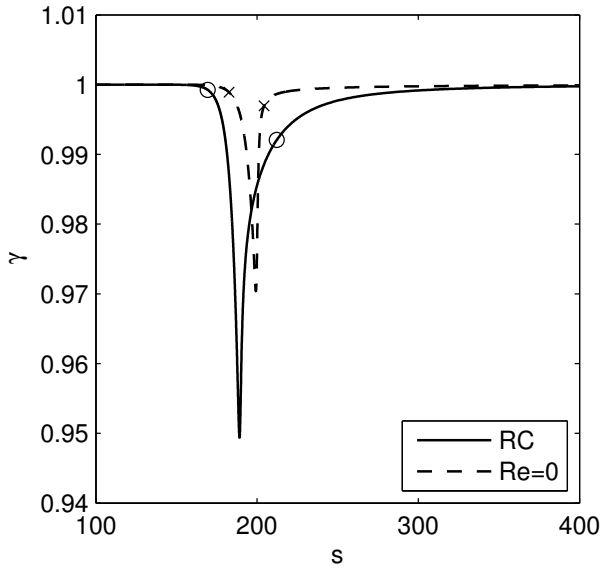

Figure 7: Dimensionless concentration of surfactant adsorbed at the interface when *Ca*=0.008 for RC and the corresponding case with *Re*=0. Circles and crosses indicate the approximate limits of the dynamic meniscus for *Re*=28.32 and *Re*=0, respectively.

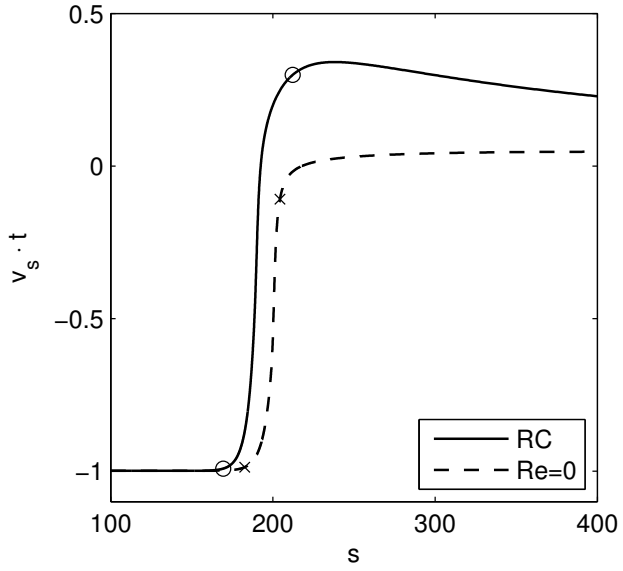

Figure 8: Interfacial surface velocity when *Ca*=0.008 for RC and the corresponding case with *Re*=0. Circles and crosses indicate the approximate limits of the dynamic meniscus for *Re*=28.32 and *Re*=0, respectively.

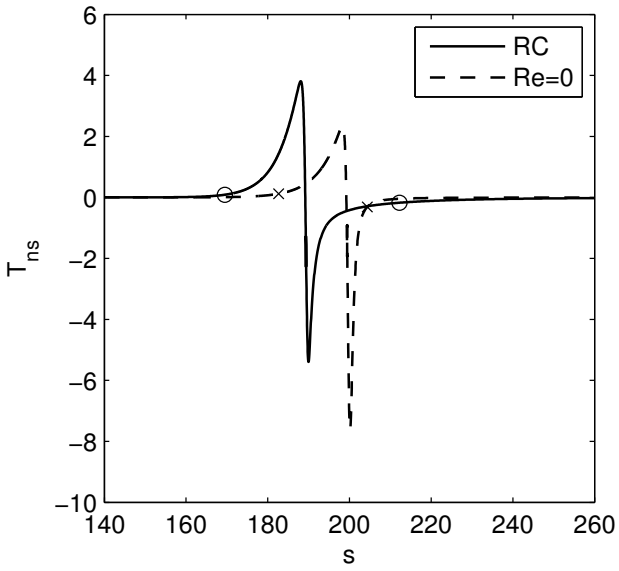

Figure 9: Marangoni stresses when *Ca*=0.008 for the RC and the corresponding case with *Re*=0. Circles and crosses indicate the approximate limits of the dynamic meniscus for *Re*=28.32 and *Re*=0, respectively.

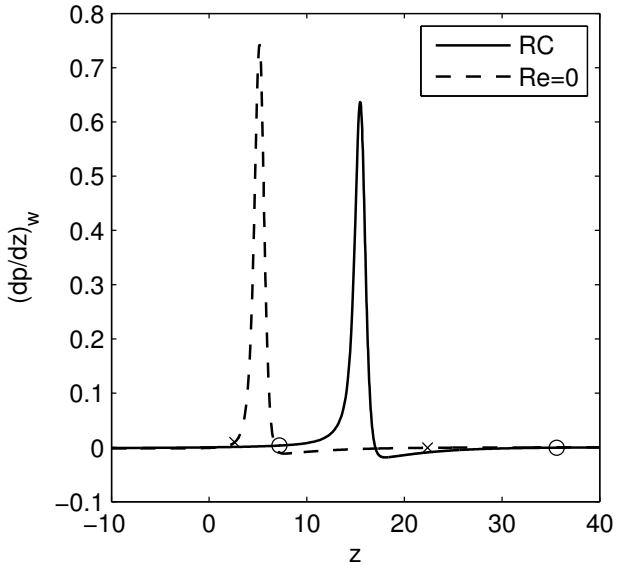

Figure 10: Dimensionless pressure gradient along the fiber wall when *Ca*=0.008 for RC and the corresponding system with *Re*=0. Circles and crosses indicate the approximate limits of the dynamic meniscus for *Re*=28.32 and *Re*=0, respectively.

In addition to the elastic forces, the film thickness results from the competition of viscous, inertia, and capillary forces. The former two drag liquid from the bath towards the film while the latter gives rise to a capillary pressure gradient which opposes to the formation of the film. Results reported in Figure 10 show the pressure gradient along the dynamic meniscus for *Re*=0 and *Re*=28.32. In both cases this gradient is positive and, hence it opposes to the flow of liquid toward the film; moreover, it is slightly smaller when inertia forces are present favoring the formation of a thicker film in contradiction with the reported values of α.

The above discussion suggests that the decrease of the thickening factor is due to the effect that inertia forces have on the Marangoni stresses. To shed some light on this issue, we evaluated the maximum and minimum values of T_{ns}, and the maximum value of $(\mathrm{d}p/\mathrm{d}z)_W$ as a function of the coating speed for RC and its counterpart with *Re*=0; results are illustrated in Figures 11 and 12; in these figures the dot corresponds to *Ca*=0.008. The curves depicted in Figure 11, show that the differences between the values of $(T_{ns})^{min}$ for the RC and *Re*=0

increase slower than the respective differences of $(T_{ns})^{max}$, as the Capillary number is augmented toward 0.008. Considering that $(T_{ns})^{min}$ is a measure of the amount of liquid pulled from the bulk toward the film while $(T_{ns})^{max}$ is a measure of the amount of liquid pulled in the opposite direction, these curves suggest that α will decrease when *Ca* approaches 0.008 from smaller values. However, for values of *Ca* larger than 0.008 the trend totally reverses indicating an abrupt increase in the values of α. =The curves of $\left(dp/dz\right)_W^{max}$ vs *Ca* (see Figure 12) are nearly equal up to *Ca*≈0.005 but for larger *Ca* values this quantity diminishes faster if inertia forces are accounted; henceforth, the pressure gradient should favor the formation of a thicker film with the increase of the coating speed when inertia is not negligible. Results reported in Figure 2 show that this is indeed the case: for values of *Ca*~0.01, the film thickness of the reference case sharply increases respect to the corresponding one with *Re*=0. The above discussion supports the suggestion that for the case under study the minimum detected in α for *Ca*=0.008 is due to the effect that inertia has on the Marangoni stresses.

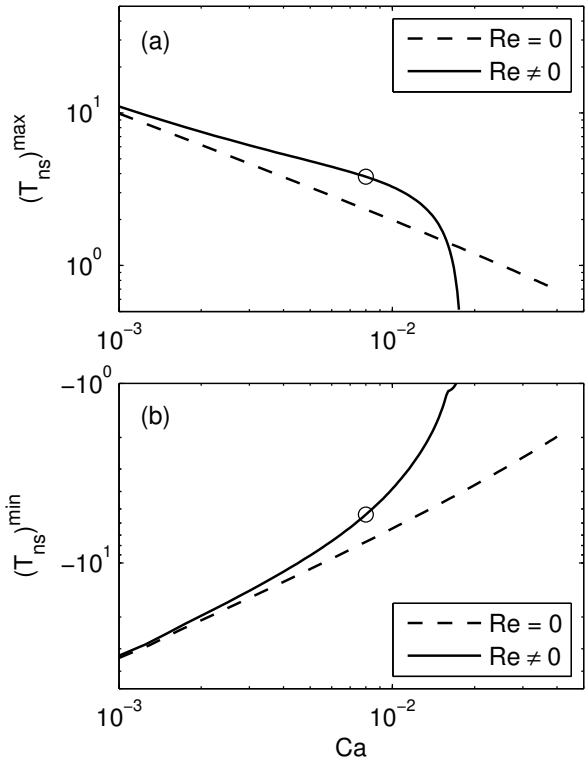

Figure 11: Influence of inertia forces on the evolution of (a) $(T_{ns})^{max}$ and (b) $(T_{ns})^{min}$ with the coating speed for the Reference case and the corresponding case with *Re*=0.

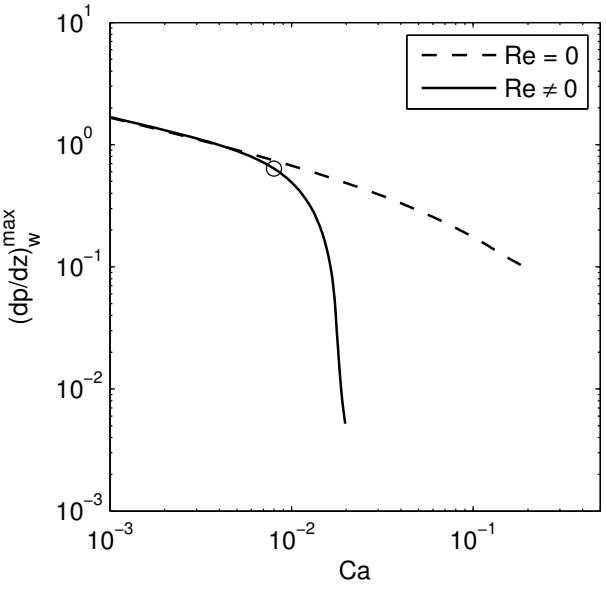

Figure 12: Influence of inertia on $(dp/dz)_W^{\max}$ for the Reference case (RC) and the corresponding case with *Re*=0.

4.3. The thickness of the entrained film. Inertial effects at different surfactant elasticities

In order to further analyze the effect that inertia forces have on the film thickness when a surface-active agent is present we carried out two numerical experiments. The first one is described in this section, the second one in section 4.4.

In the first experiment, we computed solutions when β is an order of magnitude smaller than in RC (i.e. β=0.06), being the other variables of the system those of the RC; we also computed solutions for the corresponding system with Re=0. The trends followed by the curves of h_∞ vs. Ca for β=0.06 and $Re\neq0$ or Re=0 (not illustrated here) are similar to those reported in Figure 2 for RC and RC with Re=0: also in this case a minimum in the thickening factor is detected. Nevertheless, the minimum appears at smaller Ca (0.004 instead of 0.008) and it is less noticeable; in fact, at the minimum the film thickness is 3.8% smaller than the film thickness with Re=0, while in the case portrayed in Figure 2 for β=0.6 the reduction was 15.5%. The Marangoni stresses along the dynamic meniscus as well as the pressure gradient along the wall of the fiber (not shown here) are qualitatively similar to those reported in Figures 9 and 10 for the RC, suggesting that, also for this value of β, the minimum in the thickening factor is due to the effect that inertia forces have on Marangoni stresses.

In Figure 13 we report the computed values of the film thickness as a function of the coating speed for β equal to 0, 0.06, and 0.6. It is interesting to note that the Capillary number above which the film thickness sharply thickens is —as should be expected— approximately equal to 0.017 for the three values of β considered. In the three cases the transition from the visco-capillary to the visco-inertial regime takes place when the magnitude of surface and inertia forces are comparable; that is, when the Weber number ($We=\rho V^2 b/\sigma_o$) is approximately equal to one.

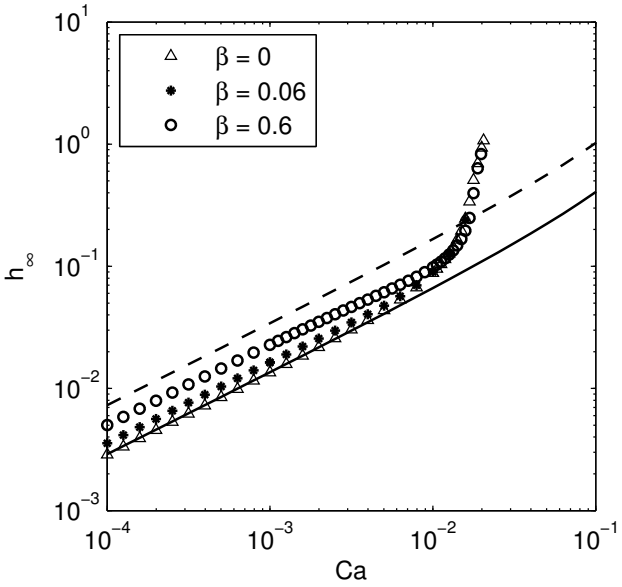

Figure 13: h_∞ vs. *Ca* for selected values of the elasticity number; the other parameters are those of the RC. The solid line corresponds to predictions of WT and the dashed one to a thickening factor $\alpha = 4^{2/3}$.

4.4. The thickness of the entrained film. Inertial effects at different surfactant solubilities

The second experiment trying to elucidate the effect of inertia on the film thickness was performed in two steps: in the first one we change the liquid viscosity to 0.01 Pa s; that is, we increase the viscosity of the RC by one order of magnitude so that the inertia effects would appear at larger *Ca* values. In addition, the relative importance of elastic effects compared to viscous ones should become weaker.

In the second step we attempt to recover the strength of the elastic forces maintaining the more viscous liquid; for that purpose we turn the surfactant rather insoluble by reducing the kinetic sorption constant by two orders of magnitude. Thus, we set $\hat{k}_a = 10^{-5}$ m/s, $k_d = 10\ s^{-1}$, and μ=0.01 Pa s, the other parameters are those of the RC.

Values of the film thickness versus *Ca* (including the two steps mentioned before) are depicted in Figure 14. Predictions identified with diamonds pertain to the first step (RC with μ=0.01 Pa s) and, as it was anticipated, the transition now occurs when *Ca*~0.17, that is when *We*~1, in agreement with the approximate analysis of Quéré and de Ryck.[8] Also, it is clear that viscous forces prevail over elastic ones since the film thicknesses are now closer to the LLD curve and the minimum in α is hardly visible.

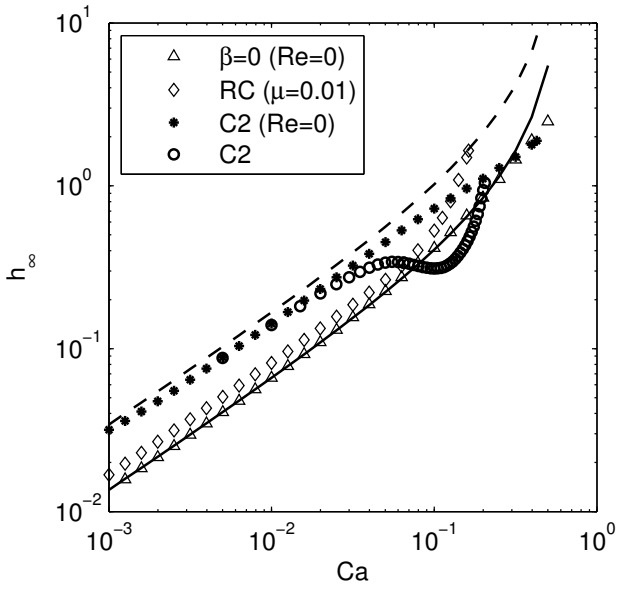

Figure 14: h_∞ vs. *Ca* for C2, for C2 and *Re*=0, and for the corresponding clean system. The solid lines are the predictions of WT and the dashed line to a thickening factor $\alpha = 4^{2/3}$.

However, in the second step where less soluble surfactants were considered, drastic changes are observed in the curve of h_∞ versus *Ca* (curve labeled C2). The adsorption time is now larger than in RC and this process is less effective to erase the concentration gradients arising from surface convection; consequently, at low coating speeds, the curve of predictions is close to the maximum thickness attainable (WT times $4^{2/3}$). As in the numerical experiments of section 4.3, the thickening factor diminishes just before the film thickness diverges due to the effect of inertia (compare the two curves labeled C2), and this reduction can be understood with the help of Figures 15 and 16 where the Marangoni traction and the

gradient of the fluid pressure along the DM, respectively, are illustrated for Ca=0.1. The analysis of the Marangoni stresses for $Re \neq 0$ and Re=0, suggests that the tendency to drag liquid toward the bulk is slightly larger when inertia forces are present. This behavior is similar to that detected in Figure 9 for the RC. However, in the present case, the reduction in α is so remarkable, that even the film thickness h_∞ decreases. This appears to have further consequences: the film thickness reduction increases the liquid pressure at the exit of the dynamic meniscus; thus, the adverse pressure gradient becomes larger and reduces the liquid flow toward the film region, which in turn reduces the film thickness even more. This negative feedback process might explain why the film thickness decreases beyond the LLD limit. Finally, as the coating speed increases, the inertia forces regain control and the film thickness increases again in the visco-inertial region.

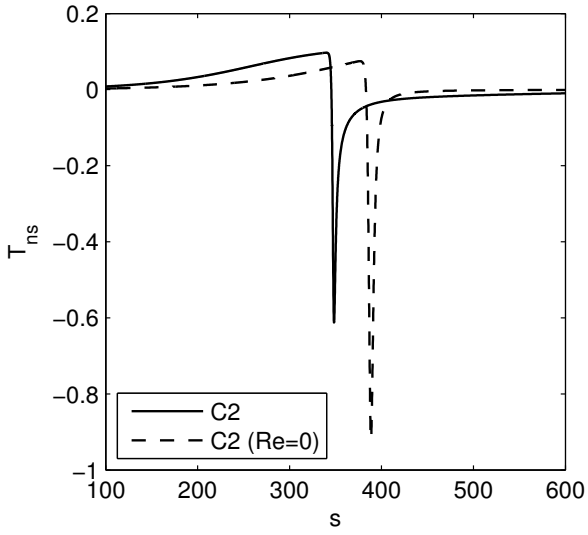

Figure 15: Marangoni stresses for case labeled C2 (with Ca=0.1) and the corresponding system with Re=0.

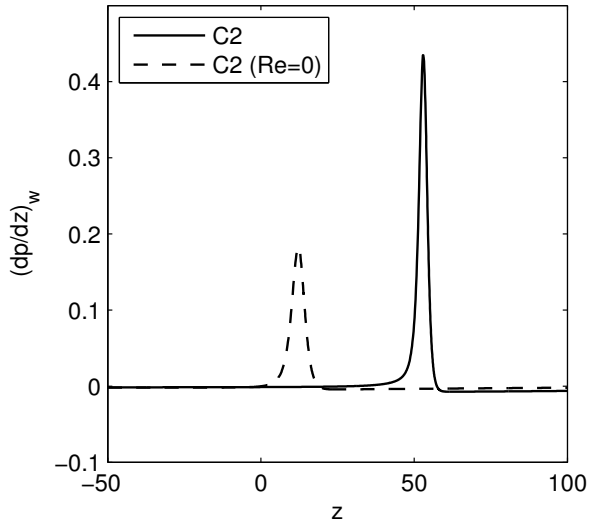

Figure 16: Dimensionless pressure distribution along the fiber wall for case labeled C2 (with *Ca*=0.1) and the corresponding one with *Re*=0.

We also evaluated the maximum and minimum T_{ns} values and the maximum value of the pressure gradient on the fiber as a function of the coating speed for C2 when *Re* is equal to or larger than zero. Trends followed by $(T_{ns})^{max}$ and $(T_{ns})^{min}$ as *Ca* is increased (not shown here) are qualitatively similar to those previously reported in Figure 11 for the RC; however, a very different behavior is observed when Figures 17 and 12 are compared: now the curve of $(dp/dz)_W^{max}$ vs. *Ca* for *Re*≠0 goes above that for *Re*=0 from *Ca*≈0.01 up to *Ca*≈0.17; moreover, the differences are quite large near the point where the minimum in α is detected.

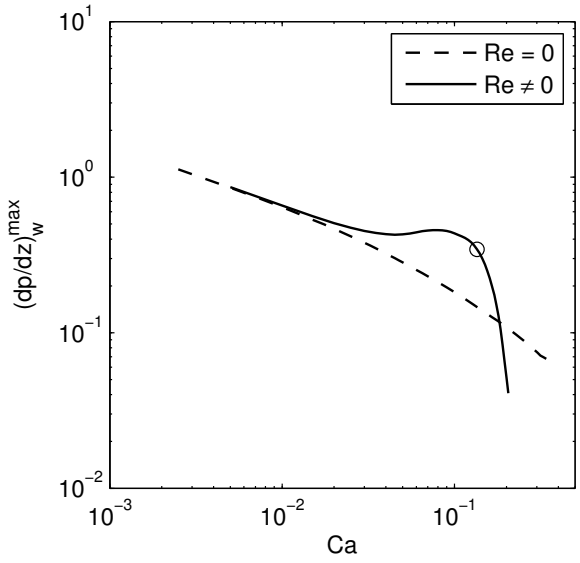

Figure 17: Influence of inertia on $(dp/dz)_W^{\max}$ for the case labeled C2 (solid line) and the corresponding case with *Re*=0 (dashed line). The dot indicates the case at which the minimum in α is detected (see Figure 14).

It is worthy to note that similar results were reported in a previous work where the effects of an insoluble surfactant on the dip coating of a planar substrate were numerically studied.[17] There, we reported that the thickness of the coated layer can be overestimated if inertia force is neglected in the computations.

Finally, in order to detect the changes induced in the flow field by the surfactant, we also computed the streamlines of the 2-D solutions numerically obtained. In a clean system, there is a streamline that intersects the free surface at a stagnation point and divides the flow domain into two regions; the streamlines pertaining to the region closer to the fiber travel into the film while the remaining ones present an inverted V shape indicating that the liquid turns around and goes back toward the bulk. However, when elastic effects are present the computed streamlines (not illustrated here) show that the stagnation point moves along the free surface away from the film; at the same time and close to the film region a second stagnation point (actually a saddle point) appears in the bulk with the

formation of a swirl that is circumvented by part of the liquid that goes into the film region. Since these changes are similar to those already reported when the effects of soluble surfactants on dip coating of plane substrates were studied,[16] they are not analyzed here.

5. CONCLUSION

Dip coating of fibers with liquids containing a soluble surfactant has been numerically analyzed. Our first goal was to compare the predictions of our numerical code with the experimental results obtained by Quéré and de Ryck[8] and by Shen et al.[10] Figures 2 and 4 show that there exists excellent agreement between predictions and experiments as long as we are in the visco-capillary regime. As the inertial effects become stronger —for values of the Capillary number larger than 0.01 in the experiments of Quéré and de Ryck[8]— the films predicted are considerably thicker than those obtained in the experiences; this discrepancy is attributed to the restraining effect that the walls of the small cylindrical tube, used as the liquid reservoir in the experiments, have on the flow motion.

Results presented by Quére and de Ryck,[8] as well as those presented by Shen et al.[10] show a non-monotonic behavior of the thickening factor (α); in fact, a minimum in α appears when the Capillary values are just before the region where the transition from the visco-capillary regime to the visco-inertial regime occurs. We used our numerical code in an effort to disclose not only the forces causing the aforementioned behavior but also the mechanisms by which they do so.

We rapidly conclude that inertia forces cause the minimum because it disappears when the film thickness predictions for the case (RC) that reproduces the experiments of Quéré and de Ryck are obtained with Re=0.[8] The mechanism by which the inertia forces act and reduce the thickening factor is not absolutely clear; however our analyses suggest that inertia forces affect the Marangoni stresses which in turn affect the film thickness.

This work, together with others we published previously, show that suitable models numerically solved can reproduce experimental results of dip coating on planar or cylindrical substrates, and with or without the presence of surfactants. However, the numerical solutions obtained are still limited to substrate speeds values below those industrially employed.

ACKNOWLEGMENT

We gratefully acknowledge the institutions ANPCyT (PICT 2012-1527), UNL (CAI+D 501 201101 00309 LI/PACT 78) and CONICET (PIP 2012-2014, 112 201101 00255), for financially supporting this work.

6. REFERENCES

(1) Schweizer, P. M.; Kistler, S. F. Liquid Film Coating. *Springer*, 1997.

(2) Landau, L.; Levich, B. Dragging of a Liquid by a Moving Plate. *Acta Physicochimica URRS* **1942**, *17*, 42.

(3) Deryagin, B. V. Thickness of Liquid Layer Adhering to Walls of Vessels on their Emptying and the Theory of Photo and Motion Picture Film Coating. *Acta Physicochimica USSR* **1943**, *39*, 13.

(4) Deryaguin, B. V. Thickness of the Liquid Film Adhering to a Moving Thread. *Dokl. Akad. Nauk USSR* **1943**, *39*, 11.

(5) Quéré, D. Fluid Coating on a Fiber. *Annu. Rev. Fluid Mech.* **1999**, *31*, 347.

(6) Quéré, D.; de Ryck, A.; Ou Ramdane, O. Liquid Coating from a Surfactant Solution. *Europhys. Lett.* **1997**, *37*, 305.

(7) Ou Ramdane, O.; Quéré, D. Thickening Factor in Marangoni Coating. *Langmuir* **1997**, *13*, 2911.

(8) Quéré, D.; de Ryck, A. Le Mouillage Dynamique des Fibres. *Ann. Phys.-Paris* **1998**, *23*, 1.

(9) Scheid, B.; Delacotte, J.; Dollet, B.; Rio, E.; Restagno, F.; Van Nierop, E. A.; Stone, H. A. The Role of Surface Rheology in Liquid Film Formation. *Europhys. Lett.* **2010**, *90*, 24002.

(10) Shen, A. Q.; Gleason, B.; McKinley, G. H.; Stone, H. A. Fibre Coating with Surfactant Solution. *Phys. Fluids* **2002**, *14*, 4055.

(11) Park, C.-W. Effects of Insoluble Surfactants on Dip Coating. *J. Colloid Interf. Sci.* **1991**, *146,* 2, 382.

(12) Carrol, B. J.; Lucassen, J. Capillarity-controlled Entrainment of Liquid by a Thin Cylindrical Filament. *Chem. Eng. Sci.* **1973**, *28,* 1, 23.

(13) Ratulowski, J.; Chang, H.-C. Marangoni Effects of Trace Impurities on the Motion of Long Bubbles in Capillaries. *J. Fluid Mech.* **1990**, *210*, 303.

(14) Krechetnikov, R; Homsy, G. M. Experimental Study of Substrate Roughness and Surfactant Effects on the Landau-Levich Law. *Physics Fluids* **2005**, *17*, 102108.

(15) Delacotte, J.; Montel, L.; Restagno, F.; Scheid, B.; Dollet, B.; Stone, H. A.; Rio, E. Plate Coating: Influence of Concentrated Surfactants on the Film Thickness. *Langmuir* **2012**, *28*, 3821.

(16) Campana, D. M.; Ubal, S.; Giavedoni, M. D.; Saita, F. A. Numerical Prediction of the Film Thickening due to Surfactants in the Landau-Levich Problem. *Phys. Fluids* **2010,** *22*, 032103-1.

(17) Campana, D. M.; Ubal, S.; Giavedoni, M. D.; Saita, F. A. A Deeper Insight into the Dip Coating Process in the Presence of Insoluble Surfactants: a Numerical Analysis. *Phys. Fluids* **2011**, *23*, 052102-1.

(18) Chang, C-H.; Franses, E. I. Adsorption Dynamics of Surfactants at the Air/Water Interface: a Critical Review of Mathematical Models, Data and Mechanisms. *Colloid. Surface. A* **1995**, *100,* 1.

(19) Campana, D. M.; Ubal, S.; Giavedoni, M. D.; Saita, F. A. Dip Coating of Fibers in the Visco-inertial Regime: Numerical Analysis. *Ind. Eng. Chem. Res.* **2013**, *52*, 12646.

(20) Campana, D. M.; Saita, F. A. Numerical Analysis of the Rayleigh Instability in Capillary Tubes. – The Influence of Surfactant Solubility. *Phys. Fluids* **2006**, *18*, 022104 1.

(21) White, D. A.; Tallmadge, A. A Theory of Withdrawal of Cylinders from Liquid Baths. *AIChE J.* **1966**, *12*, 333.

(22) Ubal, S.; Campana, D. M.; Giavedoni, M. D.; Saita, F. A. Withdrawal of a fibre from a liquid-filled capillary tube. Preliminary numerical results. Presented at the XIII Reunión sobre Recientes Avances en Física de Fluidos y sus Aplicaciones, Tandil, Argentina, November 2014.

FIGURE CAPTIONS

Figure 1: Sketch of the flow domain and coordinate system adopted.

Figure 2: Computed values of the film thickness for RC (circles), the corresponding system with *Re*=0 (asterisks), and measurements reported by Quéré & de Ryck[8] (squares). The solid line corresponds to predictions of WT and the dashed one to a thickening factor $\alpha = 4^{2/3}$.

Figure 3: Film thickening factor as a function of the radius of the fiber for two values of the adsorption constant; other parameters are those of the reference case. The squares indicate the experiments of Quéré and de Ryck.[8]

Figure 4: Comparison between numerical predictions (circles) and the measurements by Shen et al. (squares).[10] The solid line corresponds to predictions of WT and the dashed one to a thickening factor $\alpha = 4^{2/3}$.

Figure 5: Shapes of the menisci for RC (and *Ca*=0.008) and the corresponding system with *Re*=0. Circles and crosses indicate the approximate limits of the dynamic meniscus for *Re*=28.32 and *Re*=0, respectively.

Figure 6: Dimensionless interfacial pressure along the free surface when *Ca*=0.008 for RC and the corresponding case with *Re*=0. Circles and crosses indicate the approximate limits of the dynamic meniscus for *Re*=28.32 and *Re*=0, respectively.

Figure 7: Dimensionless concentration of surfactant adsorbed at the interface when *Ca*=0.008 for RC and the corresponding case with *Re*=0. Circles and crosses indicate the approximate limits of the dynamic meniscus for *Re*=28.32 and *Re*=0, respectively.

Figure 8: Interfacial surface velocity when *Ca*=0.008 for RC and the corresponding case with *Re*=0. Circles and crosses indicate the approximate limits of the dynamic meniscus for *Re*=28.32 and *Re*=0, respectively.

Figure 9: Marangoni stresses when *Ca*=0.008 for the RC and the corresponding case with *Re*=0. Circles and crosses indicate the approximate limits of the dynamic meniscus for *Re*=28.32 and *Re*=0, respectively.

Figure 10: Dimensionless pressure gradient along the fiber wall when *Ca*=0.008 for RC and the corresponding system with *Re*=0. Circles and crosses indicate the approximate limits of the dynamic meniscus for *Re*=28.32 and *Re*=0, respectively.

Figure 11: Influence of inertia forces on the evolution of (a) $(T_{ns})^{\max}$ and (b) $(T_{ns})^{\min}$ with the coating speed for the RC and the corresponding case with *Re*=0.

Figure 12: Influence of inertia on $\left(dp/dz\right)_W^{\max}$ for the RC and the corresponding case with *Re*=0.

Figure 13: h_∞ vs. *Ca* for selected values of the elasticity number; the other parameters are those of the RC. The solid line corresponds to predictions of WT and the dashed one to a thickening factor $\alpha = 4^{2/3}$.

Figure 14: h_∞ vs. *Ca* for C2, for C2 and *Re*=0, and for the corresponding clean system. The solid lines are the predictions of WT and the dashed line to a thickening factor $\alpha = 4^{2/3}$.

Figure 15: Marangoni stresses for case labeled C2 (with *Ca*=0.1) and the corresponding system with *Re*=0.

Figure 16: Dimensionless pressure distribution along the fiber wall for case labeled C2 (with *Ca*=0.1) and the corresponding one with *Re*=0.

Figure 17: Influence of inertia on $\left(dp/dz\right)_W^{\max}$ for the case labeled C2 (solid line) and the corresponding case with *Re*=0 (dashed line). The dot indicates the case at which the minimum in α is detected (see Figure 14).

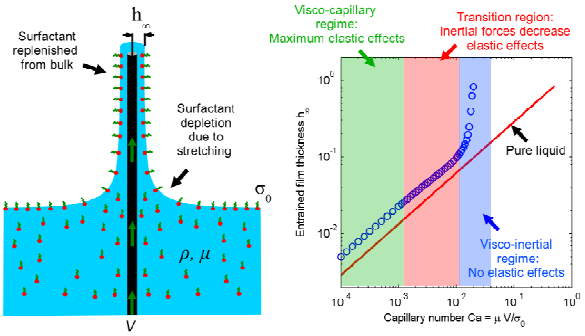

For Table of Contents Only